VOL 65 NO 776 AUGUST 1992

The British Journal of Radiology

Contents

Case of the month

Correspondence

Proceedings

Book reviews

 Published by The British Institute of Radiology, 36 Portland Place, London W1N 4AT. Origination by BPCC Whitefriars Ltd, Tunbridge Wells, and printed and bound in Great Britain by BPCC Wheatons Ltd, Exeter.
ISSN 0007 1285

1992, *The British Journal of Radiology, 65*, 653–661

Direct and CT measurements of canals and foramina of the skull base

By *A. Berlis, R. Putz, MD and *M. Schumacher, MD

Anatomische Anstalt, Ludwig-Maximilians-Universität Müchen, Pettenkoferstrasse 11, D-8000 München and *Abteilung Röntgendiagnostik, Sektion Neuroradiologie, Albert-Ludwigs-Universität Freiburg i.Br., D-7800 Freiburg i.Br., Hauptstrasse 5, Germany

(*Received 9 July 1991 and in revised form 20 November 1991, accepted 14 January 1992*)

Keywords: Skull base, CT, Foramen, Canal, Fissure

Abstract. This investigation is based on measurements of 60 macerated adult European skulls from the Alexander-Ecker Collection at the Anatomy Department of the University of Freiburg. Computer tomographical (CT) and anatomical measurements were compared to assess the accuracy of the CT representation of osseous structures. Nine structures were examined: the optic canal; the superior orbital fissure; the foramen rotundum; the foramen ovale; the foramen spinosum; the foramen Vesalii (venosum); the carotid canal; the internal auditory canal, and the hypoglossal canal. The results show a good and even excellent correlation if the cranial opening is approximately at a right angle to the scanline. For this reason, the results of the coronal examination of the internal auditory canal are less satisfactory, and the coronal and axial measurements of the hypoglossal canal show only a moderately good correlation.

Knowledge of the normal and variant positions of the canals and foramina of the skull base is important for radiologists, neurosurgeons and anatomists, because of the increasingly refined techniques available. Although the effectiveness of computed tomography (CT) in diagnosing bony lesions is uncontested, most of the authors describe optimal positioning without mentioning the correlation between their findings and the actual anatomical position of the osseous structures referred to at the time of writing. CT measurements of the position of the internal auditory porus (Heller et al, 1983), the internal auditory canal (Silverstein et al, 1988) and the foramen Vesalii (venosum) (Lanzieri et al, 1988) are available. Only Silverstein et al (1988), however, have assessed the correlation between CT measurements and those taken from dissections of the temporal bone.

In the following study, anatomical and CT measurements, including length, breadth and height of optic canals, superior orbital fissure, foramen rotundum, foramen ovale, foramen spinosum, foramen Vesalii (venosum), carotid canal, internal auditory canal, and hypoglossal canal, and the distances between these structures, are evaluated. The extent to which anatomical variations can be assessed by CT has also been investigated.

Material and methods

A total of 60 macerated adult European skulls from the Alexander-Ecker Collection at the Anatomy Department of the University of Freiburg were studied.

For the direct anatomical measurements we used digital internal callipers (Mitutoyo 526–153/526–163: 1.50–7.30 $\pm$ 0.01 mm), a digital measuring instrument (Mitutoyo 500–110: 0–150 $\pm$ 0.02 mm), an anthropometric instrument (Berlis, 1990) of our own construction (0–260 $\pm$ 1 mm) and a tintack with a millimetre rule ($\pm$ 1 mm).

The CT scans of the skull base were obtained using a Siemens Somatom DR-H. Continuous 1 mm sections were taken at angles of 10° (axial projection) and 70° (coronal projection) to the radiographic baseline (RB) (Reid's baseline or anthropological baseline). The CT number range was viewed at a window width of 4000 HE. The exposure factors were 550 mA and 125 kV with a scan speed of 9.6 s. The skulls were positioned in plastic on a table and the scanlines were defined by Topo-scan. Double measurements were recorded directly on the monitor using a joystick.

Results

Optic canal (Figs 1 & 8). Following Lang (1981), we divided this canal into three parts: an orbital part (an elongated oval on section), a middle part or "optic waist" (Lang & Oehmann, 1976) and an intracranial part. The mean angle of the axis of the canal and the sagittal plane (SP) was 39.1°, and the RB was −15.5°. This means that the coronal sections met the canal at an angle of 85.5°.

Several variants show asymmetry in the shape of the canal. The so-called keyhole anomaly (Fig. 1) is a result of the absence of the floor at the cranial opening (Potter & Trokel, 1971). This anomaly appears in 3.3% of our material. Another variant is the figure-of-eight optic canal, with a separate canal for the ophthalmic artery produced by a spicule of bone uniting the roots of the lesser wing of the sphenoid. This appeared as a duplicate cranial opening with lengths of 3.0, 2.5 or 1.6 mm and a thickness of 1.4, 1.7 or 1.5 mm. The lumen measured 2.11 × 1.55, 1.76 × 1.00 or 2.50 × 2.00 mm, and

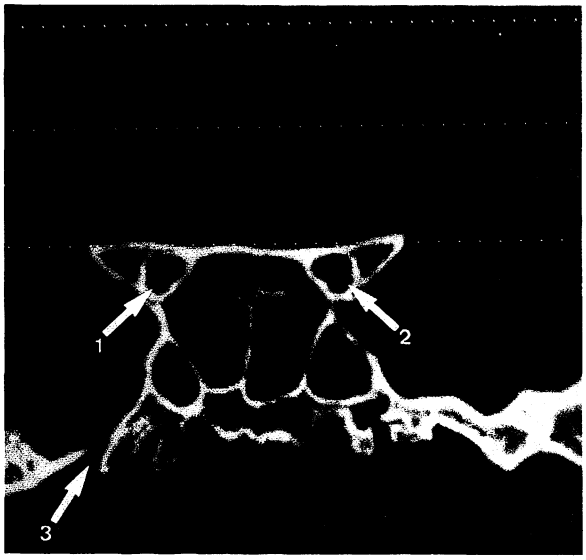

Figure 1. Coronal projection of the optic canal of the skull 42/351. A separate passage for the ophthalmic artery appears on both sides of the skull. 1 = Right optic canal—it appears to be a "keyhole" anomaly, but its "figure-of-eight" character can be seen at a deeper level; 2 = left optic canal of "keyhole" type and 3 = foramen ovale.

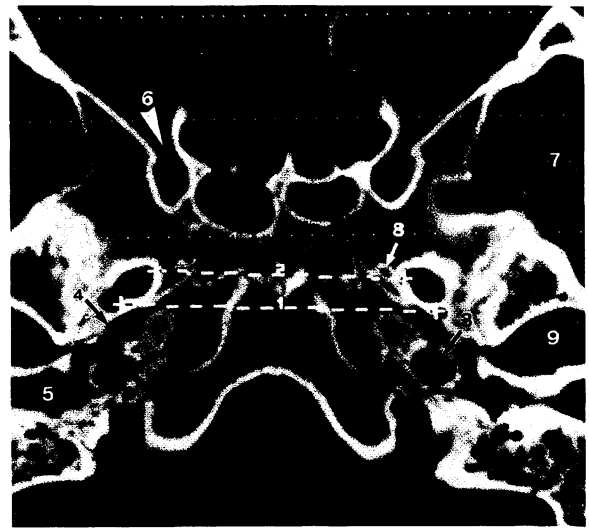

Figure 2. Axial projection of the skull base. 1 = Measuring line between foramina ovalia; 2 = measuring line between foramina spinosa; 3 = carotid canal; 4 = pharyngotympanic tube; 5 = external auditory meatus; 6 = inferior orbital fissure; 7 = middle cranial fossa; 8 = foramen Vesalii and 9 = mandibular fossa.

had an incidence of 2.5% (individual measurements in Table I).

Superior orbital fissure. The superior orbital fissure was explored in coronal projection and could be seen in its entirety (individual measurements in Table II).

Foramen rotundum. The foramen rotundum is, in spite of its name, a short oval canal in the antero-medial portion of the greater sphenoidal wing. According to Lang (1981), the axis lies at a mean angle of $-14°$ to the RB and at 15° to the SP. Consequently, the canal appears in coronal section at an angle of 84° (individual measurements in Table III).

Foramen ovale (Fig. 2). According to Honda et al (1987), the optimal CT plane lies between 0° and 20° to the RB and the foramen can be seen using CT on axial projection. We found the shape of the foramen ovale to be truly oval (56.7%), an elongated oval (31.7%) or semicircular (11.7%). In our material we found two variations in shape. In 12.5% of cases the foramen was partially divided by a thin bony spicule and in one case (0.8%) it was duplicated (individual measurements in Table IV).

Foramen spinosum (Fig. 2). Honda et al (1987) describe the axial projection as a good position for CT examination of this foramen. We found that in 0.8% of cases the foramen spinosum was absent and the foramen ovale was of normal size and shape (individual measurements in Table V).

Foramen Vesalii (or venosum) (Fig. 2). This foramen transmits a small vein connecting the cavernous sinus with the pterygoid venous plexus. According to Lang (1981), the foramen Vesalii is located in the greater sphenoidal wing posterior to the foramen rotundum. In most cases it is postero-medial, and in a few cases postero-lateral, to the foramen rotundum. In 25% of cases we found the foramen on the right side, in 35% on the left side, bilaterally in 15% and completely absent in 64%. The foramen Vesalii was examined in axial projection (individual measurements in Table VI).

Carotid canal (Figs 2 & 3). Following Teufel (1964),

Figure 3. Coronal projection of the carotid canal showing the extracranial aperture and the ascending petrous portion, with the petrous curvature. 1 = Breadth at the petrous curvature; 2 = height at the petrous curvature and 3 = mastoid part of facial canal.

Table I. Measurements of the optic canal ($n = 120$)

		Mean (mm)	Range (mm)	Standard deviation (SD) (mm)	r^a
Orbital part					
Transverse diameter	CT/70°	5.66	4–10	1.10	0.56
	Skull	4.75	3.40–5.69	0.54	
Vertical diameter	CT/70°	5.01	3–7	0.55	0.53
	Skull	5.46	3.89–7.28	0.54	
Distance of lateral margins	CT/70°	32.83	27–40	2.76	0.73
	Skull	33.13	27.96–40.86	2.77	
Distance of medial margins	CT/70°	20.95	15–30	2.99	—
	Skull	—	—	—	
Optic waist					
Transverse diameter	CT/70°	6.43	4–9	1.08	0.61
	Skull	4.39	3.21–5.47	0.48	
Vertical diameter	CT/70°	5.01	3–7	0.68	0.45
	Skull	4.69	3.04–6.35	0.58	
Intracranial part					
Transverse diameter	CT/70°	7.64	5–11	1.11	0.48
	Skull	6.25	4.21–8.49	0.90	
Vertical diameter	CT/70°	3.63	3–9	0.55	0.73
	Skull	3.70	2.60–5.53	0.60	
Distance of lateral margins	CT/70°	27.97	24–33	2.34	0.73
	Skull	25.15	19.83–30.87	2.51	
Distance of medial margins	CT/70°	12.93	8–19	2.54	0.83
	Skull	14.12	9.35–22.26	2.36	

[a] r = Correlation coefficient between direct measurements and CT measurements. (This applies to Tables I–IX.)

we divided the carotid canal into an ascending petrous portion (with the petrous curvature) (Fig. 3), a transverse petrous portion and an ascending cavernous portion. According to Lang et al (1983), the ascending petrous portion encounters the RB at an angle of 80.9° and can therefore be seen in the coronal projection. The horizontal or transverse portion can be seen in the axial projections (individual measurements in Table VII).

Internal auditory canal (Figs 4 & 5). The axis of the canal lies at an angle of $90° \pm 6°$ to the SP (Hassmann, 1975). Because of this "right angle", and because of the frontal orientation of its course in the petrous bone, the canal is best seen in coronal projection (Köster, 1988). The canal, which appears in axial (CT/10°) and coronal (CT/70°) scans, begins at the porus as an oval expanded orifice in the petrous portion of the temporal bone and ends with the falciform crest at the fundus.

The height of the porus, the canal and the fundus, and the length and the distances between the superior and inferior margins on the two sides, can be seen in

Table II. Measurements of the superior orbital fissure ($n = 120$)

		Mean (mm)	Range (mm)	SD (mm)	r
Length	CT/70°	20.05	13–25	2.72	0.56
	Skull	20.05	12.21–25.29	2.61	
Distance of lateral margins	CT/70°	56.53	46–72	4.65	0.90
	Skull	56.41	45.04–66.57	4.42	
Distance of medial margins	CT/70°	33.00	27–41	3.34	0.95
	Skull	32.81	27.61–40.01	3.29	
Shortest distance	CT/70°	28.20	23–36	2.78	0.93
	Skull	28.18	22.89–36.85	3.08	

Table III. Measurements of the foramen rotundum (n = 120)

		Mean (mm)	Range (mm)	SD (mm)	r
Breadth	CT/70°	3.11	2–5	0.78	0.69
	Skull	3.29	2.05–5.14	0.63	
Height	CT/70°	3.13	2–5	0.56	0.61
	Skull	3.09	2.08–5.05	0.69	
Intracranial distance	CT/70°	33.00	27–41	3.50	0.98
	Skull	33.39	26.84–41.92	3.63	

Table IV. Measurements of the foramen ovale (n = 120)

		Mean (mm)	Range (mm)	SD (mm)	r
Breadth	CT/10°	4.20	2–6	0.87	0.75
	Skull	3.91	2.44–6.66	0.77	
Length	CT/10°	7.67	5–12	1.43	0.89
	Skull	7.41	4.61–11.29	1.31	
Distance	CT/10°	44.47	35–59	4.17	0.98
	Skull	45.38	35.36–60.63	4.12	

Table V. Measurements of the foramen spinosum (n = 119)

		Mean (mm)	Range (mm)	SD (mm)	r
Breadth	CT/10°	1.86	1–4	0.60	0.61
	Skull	2.07	1.23–2.82	0.28	
Length	CT/10°	2.42	1–4	0.71	0.61
	Skull	2.60	1.53–4.35	0.52	
Distance	CT/10°	58.29	48–68	4.28	0.98
	Skull	58.42	48.85–67.61	4.15	

Table VI. Measurements of the foramen Vesalii (or venosum) (n = 36)

		Mean (mm)	Range (mm)	SD (mm)	r
Breadth	CT/10°	1.04	1–2	0.13	0.25
	Skull	1.33	1.00–2.04	0.35	
Length	CT/10°	1.68	1–3	0.68	0.54
	Skull	1.79	1.00–3.46	0.68	
Distance	CT/10°	35.36	30–42	3.72	0.83
	Skull	36.09	29.25–43.09	3.97	

Table VII. Measurements of the carotid canal (n = 120)

		Mean (mm)	Range (mm)	SD (mm)	r
Axial projection					
Breadth of extracranial aperture	CT/10°	5.88	3–8	0.64	0.66
	Skull	5.69	3.66–7.05	0.35	
Length of extracranial aperture	CT/10°	7.91	5–12	1.13	0.75
	Skull	7.81	4.45–12.41	1.16	
Extracranial distance	CT/10°	49.88	38–62	4.91	0.95
	Skull	50.58	37.82–62.37	4.77	
Length of horizontal portion	CT/10°	26.97	21–35	2.53	0.85
	Skull	27.90	21.67–35.51	2.52	
Coronal projection					
Length of ascending petrous part	CT/70°	11.10	7–15	1.61	0.57
	Skull	9.49	6–13	1.51	
Length of petrous curvature	CT/70°	6.33	4–8	0.79	
Breadth of petrous curvature	CT/70°	35.36	30–42	3.72	

coronal projection. The length and breadth of the porus, the canal and the fundus, and the distance between the anterior and posterior margins, are better seen in the axial projections (Fig. 4) (individual measurements in Table VIII).

Hypoglossal canal (Figs 6 & 7). The axis of the canal meets the SP at an angle of 44.9° (Schmidt, 1975) and the RB at an angle of −7° (Kirdani, 1967). The canal is seen on both axial (CT/10°) and coronal (CT/70°) scans. The measurement of the height and distance between the inferior and superior margins can be seen on coronal projection. The measurement of breadth, length and distance between the anterior and posterior margins on the two sides is seen on the axial projections. We found that 11.6% were partially divided on the right side and 15% on the left. A complete division into two parts was encountered in 16% (right) and in 10% (left). Complete bilateral division was found in only 3.3% of cases (individual measurements in Table IX).

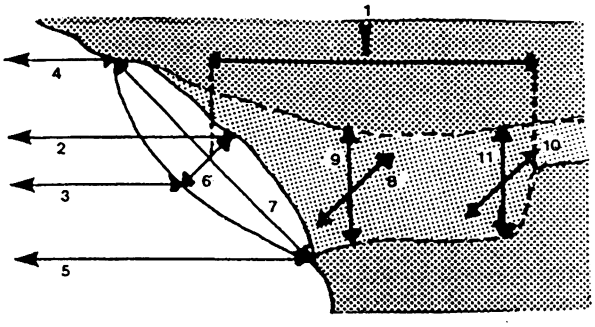

Figure 4. Internal auditory canal including measuring lines between the two sides of the skull (modified from Lang, 1981). 1 = Length of canal; 2 = distance between superior margins; 3 = distance between inferior margins; 4 = distance between anterior margins; 5 = distance between posterior margins; 6 = breadth of the porus; 7 = length of the porus; 8 = breadth of the canal; 9 = height of the canal; 10 = breadth of the fundus and 11 = height of the fundus.

Discussion

Recent advances in CT have produced a growing need for precise information about optimal scanning positions for examining the morphological and metrical details of the foramina and canals in the base of the skull. This study is an attempt to compare CT examina-

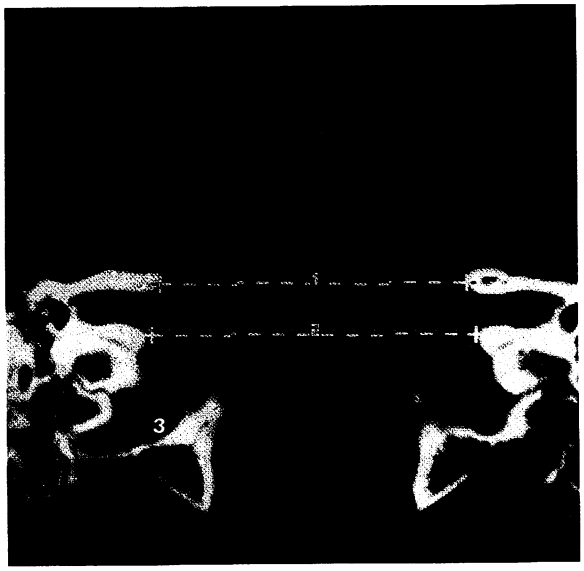

Figure 5. Coronal projection of the internal auditory canal. 1 = Distance between the superior margins; 2 = distance between the inferior margins and 3 = sigmoid sulcus.

Table VIII. Measurements of the internal auditory canal (n = 120)

		Mean (mm)	Range (mm)	SD (mm)	r
Height of porus	CT/70°	8.05	5–15	1.84	0.27
	Skull	4.77	2.62–8.71	1.00	
Breadth of porus	CT/10°	8.91	5–13	1.72	0.65
	Skull	9.57	6.72–12.90	1.53	
Height of canal	CT/70°	3.95	2–6	0.75	0.51
	Skull	3.70	2.21–5.69	0.71	
Breadth of canal	CT/10°	3.87	2–6	0.80	0.60
	Skull	4.11	2.35–6.36	0.69	
Height of fundus	CT/70°	4.33	3–7	0.92	
Breadth of fundus	CT/10°	3.34	2–5	0.79	
Length of canal	CT/70°	11.98	9–17	1.60	0.61
	Skull	11.68	8–15	1.50	0.55
	CT/10°	10.38	7–14	1.47	
Distance of superior margins	CT/70°	46.05	37–59	4.67	0.82
	Skull	41.42	42.85–62.35	4.81	
Distance of inferior margins	CT/70°	46.30	33–58	5.29	0.77
	Skull	50.48	40.08–59.48	5.02	
Distance of anterior margins	CT/10°	44.66	36–55	4.21	0.90
	Skull	44.43	36.50–53.93	4.13	
Distance of posterior margins	CT/10°	57.47	45–67	4.73	0.98
	Skull	57.57	45.49–66.69	4.82	

tion at two appropriate CT angles with direct measurements made on the macerated skull. Comparison of the two methods allows the accuracy of CT to be assessed and the best angles for viewing the skull to be determined. According to Radü et al (1987), CT examination of small structures is made impossible by the partial volume effect. Against this, Köster (1988) claims that the increased spatial resolution of CT has overcome this difficulty. However, because of this uncertainty, only a few publications listing CT measurements of these foramina and canals have so far appeared (Heller et al, 1983; Silverstein et al, 1988; Lanzieri et al, 1988).

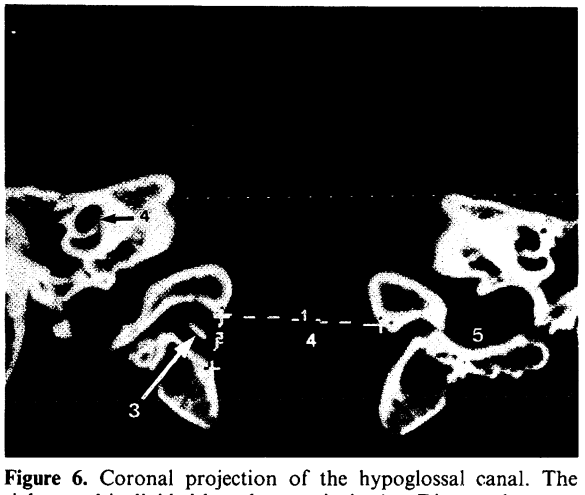

Figure 6. Coronal projection of the hypoglossal canal. The right canal is divided by a bony spicule. 1 = Distance between the superior margins of the porus internus; 2 = height of the porus internus; 3 = bony spicule; 4 = cochlea and 5 = jugular fossa.

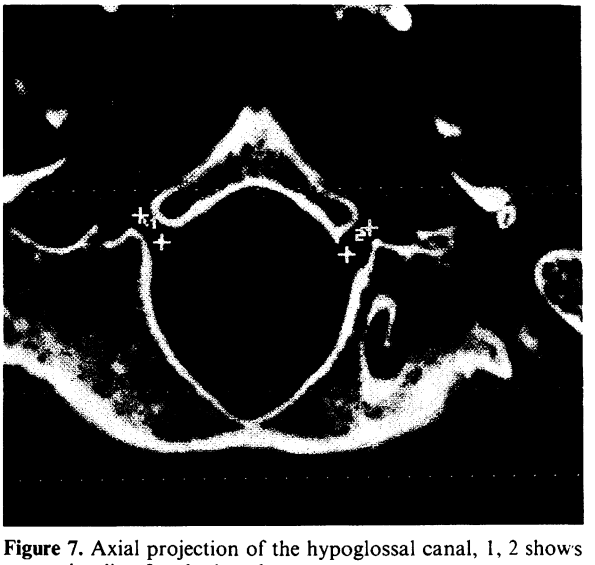

Figure 7. Axial projection of the hypoglossal canal, 1, 2 shows measuring line for the length.

Table IX. Measurements of the hypoglossal canal ($n = 120$)

		Mean (mm)	Range (mm)	SD (mm)	r
Porus internus					
Height	CT/70°	9.08	5–14	1.88	0.24
	Skull	5.41	2.75–12.08	1.58	
Breadth	CT/10°	6.85	3–11	1.69	0.31
	Skull	8.00	3.97–13.39	1.74	
Distance of superior margins	CT/70°	24.39	20–31	2.50	0.69
	Skull	29.30	22.98–35.94	2.93	
Distance of inferior margins	CT/70°	25.97	19–32	2.67	0.56
	Skull	27.21	18.40–33.14	3.22	
Distance of anterior margins	CT/10°	24.63	20–32	2.43	0.76
	Skull	24.38	19.47–32.51	2.42	
Distance of posterior margins	CT/10°	31.98	25–39	3.16	0.88
	Skull	31.95	26.01–38.08	2.70	
Canal					
Height	CT/70°	4.50	3–7	0.84	0.47
	Skull	3.57	2.24–5.28	0.69	
Breadth	CT/10°	4.24	2–8	1.06	0.44
	Skull	5.02	2.29–7.06	1.03	
Length	CT/10°	7.58	4–11	1.61	0.61
	Skull	7.78	5–12	1.46	
Porus exturnus					
Height	CT/70°	9.08	5–15	2.04	0.22
	Skull	5.70	3.14–8.41	1.12	
Breadth	CT/10°	6.95	3–13	1.61	0.40
	Skull	8.01	3.58–13.69	1.97	
Distance of superior margins	CT/70°	40.05	31–50	4.38	0.45
	Skull	43.14	30.08–51.22	3.71	
Distance of inferior margins	CT/70°	44.57	36–54	4.04	0.64
	Skull	38.91	30.61–47.55	3.71	
Distance of anterior margins	CT/10°	33.50	28–39	3.74	0.90
	Skull	34.00	28.43–39.36	2.53	
Distance of posterior margins	CT/10°	44.38	36–53	3.74	0.76
	Skull	45.50	37.36–56.45	4.48	

There are three main sources of error. First, there is no clinically acceptable plane corresponding to both axes of canals and foramina, and the actual position chosen must therefore represent a compromise. The problems of attaining exact representation and the differences between the two methods of measurement are illustrated by examples taken from the optical canal (Fig. 8). Secondly, there is a greater margin of error to be expected with CT (± 0.5 mm) than with direct manual measurement (± 0.01 mm). Finally, there is the partial volume effect, which should however have relatively little significance in this study, since sections of 1 mm were used. Furthermore, it will only be operative if the structures are not exactly perpendicular to the scan.

The coronal projection of the optic canal proved to be ideal for CT examination, correlation of direct measurements with CT measurements of the vertical diameters were good, but those of the transverse diameters were poor. This is because the direct measurement is made perpendicular to the course of the canal, whereas the CT measurement is perpendicular to the SP (Fig. 8).

Finally, a qualitative assessment of the correlation between the two methods of measurement and the representation of the canals and foramina at each projection is shown in Table X.

These results show that modern high resolution CT, with 1 mm sections, provides precise measurements which differ little from the actual distances in the anatomical specimen. It is to be assumed, however, that the canals and foramina lie perpendicular to the scanline.

The axial projection is optimal for the foramen ovale,

Table X. Representation of foramina and canals of the skull base, and correlation of direct measurements of breadth, height and length with the corresponding values obtained using CT in coronal (70°) and axial (10°) projection

	Correlation direct and CT/10°	Representation in CT/10°	Correlation direct and CT/70°	Representation in CT/70°
Optic canal			$++^{v}$	$+++^{v}$
			$+^{t}$	$+++^{t}$
Superior orbital fissure			++	+++
Foramen rotundum			++	++
Foramen ovale	+++	+++		
Foramen spinosum	++	++		
Foramen Vesalii	+	++		
Carotid canal	++	+++	++	+++
Internal auditory canal	++	+++	+	+++
Hypoglossal canal	+	+++	+	+++

+ = poor ($r < 0.50$), ++ = good ($r = 0.51$–0.75), +++ = excellent ($r > 0.76$).
^{v}vertical diameter, ^{t}transverse diameter.

the foramen spinosum, the foramen Vesalii, the horizontal part of the carotid canal and the internal auditory canal, whereas the coronal projection is suitable for the optic canal, the superior orbital fissure, the foramen rotundum and the ascending part of the carotid canal.

A comparison of the derived measurements of the coronal projection of the internal auditory canal, and both projections of the hypoglossal canal, with direct measurement is not possible because of the different measuring lines. Owing to the frontal orientation of its course in the petrous temporal bone, the internal auditory canal is best represented in coronal projection. A good quality picture of the hypoglossal canal can be obtained with coronal projection, whereas the axial projection has the alternative advantage of showing the whole extent of its course.

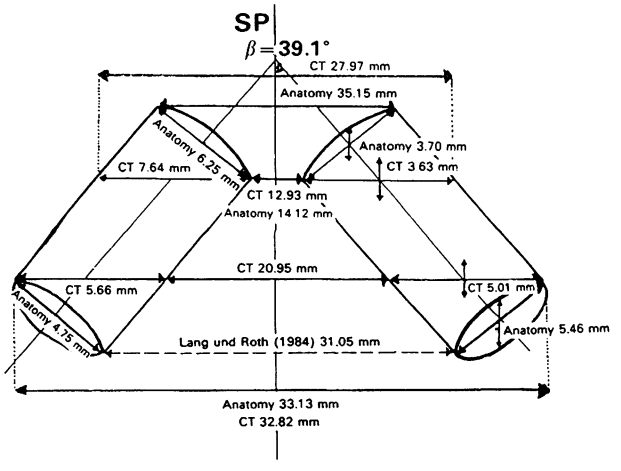

Figure 8. Model of the optic canal showing measuring lines. Difference between the direct and CT measurement is due to the different directions of the measuring lines.

Acknowledgments

We would like to express our thanks to the Wissenschaftliche Gesellschaft of Freiburg i. Br, whose support made this investigation possible, and to Dr Francis Steel for reading the manuscript.

References

BERLIS, A., 1990. Korrelation anatomischer und computertomographischer Maße von Kanälen und Foramina der Schädelbasis. *Medizinische Dissertation Freiburg* i. Br.

HASSMANN, H., 1975. *Form, Maße und Verläufe der Schädelkanäle: Canalis infraorbitalis, Canalis incisivus, Canalis palatinus major, Foramen spinosum und Meatus acusticus internus.* Medizinische Dissertation Würzburg.

HELLER, M., MÖHRLE, M., JEND, H. H., HÖRMANN, K., HELMKE, K., 1983. Anssagekraft der CT in der Diagnostik von Tumoren der Kleinhirnbrückenwinkelregion. *Röfo, 139,* 48–55.

HONDA, H., WATANABE, K., KUSOMOTO, S., HOSHI, H., NISHIKAWA, K., KAHITSUBATA, Y., JINNOUCHI, S., KODAMA, T., NAKAYAMA, S. & ONO, S., 1987. Optimal positioning for CT examinations of the skull base. Experimental and clinical studies. *European Journal of Radiology, 7,* 225–228.

KIRDANI, M. A., 1967. The normal hypoglossal canal. *American Journal of Roentgenology, 99,* 700–704.

KÖSTER, O., 1988. *CT des Felsenbeines* (Thieme Verlag, Stuttgart, New York).

LANG, J., 1981. *Klinische Anatomie des Kopfes* (Springer-Verlag Berlin, Heidelberg, New York).

LANG, J. & OEHMANN, G., 1976. Formentwicklung des Canalis opticus, seine Maße und Einstellung zu den Schädelebenen. *Verhandlungen der Anatomischen Gesellschaft, 70,* 567–574.

LANG, J., SCHAFHAUSER, O. & HOFFMANN, S., 1983. Über die postnatale Entwicklung der transbasalen Schädelpforten: Canalis caroticus, Foramen jugulare, Canalis hypoglossalis, Canalis condylaris, Foramen magnum. *Anatomischer Anzeiger, 153,* 315–357.

LANZIERI, C. F., DUCHESNEAU, P. M., ROSENBLOOM, S. A., SMITH, A. S. & ROSENBAUM, A. E., 1988. The significance of asymetry of the foramen Vesalius. *American Journal of Neuroradiology, 9,* 1201–1204.

POTTER, G. D. & TROKEL, S. L., 1971. In Radiology of the

Skull and Brain. The Skull, ed. by Th. H. Newton and G. D. Potts (C.V. Mosby Company, Saint Louis), pp. 487–506.

RADÜ, E. W., KENDALL, B. E. & MOSELEY, I. F., 1987. *Computertomographie des Kopfes.* (Thieme-Verlag, Stuttgart, New York).

SCHMIDT, Th., 1975. *Der Canalis hypoglossus: Topographie, Form, Länge, Durchmesser und Volumen.* Medizinische Dissertation Würzburg.

SILVERSTEIN, H., NORRELL, H., SMOUHA, E. & HABERKAMP, T., 1988. The singular canal: A valuable landmark in surgery of the internal auditory canal. *Otolaryngology—Head and Neck Surgery, 98,* 138–143.

TEUFEL, J., 1964. Einbau der Arteria carotis interna in den Canalis caroticus unter Berücksichtigung des transversalen Venenabflusses. *Morphologisches Jahrbuch, 106,* 188–274.